HIGH-TEMPERATURE EXPERIMENTAL CHARACTERISATION OF XN40F FOR LIFE PREDICTION OF SPF TOOLS

A. A. Deshpande, S.B. Leen, T.H. Hyde

HIGH-TEMPERATURE EXPERIMENTAL CHARACTERISATION OF XN40F FOR LIFE PREDICTION OF SPF TOOLS

A. A. Deshpande[1], S B Leen[2], T H Hyde[3]
School of Mechanical, Materials & Manufacturing Engineering, University of Nottingham, NG7 2RD, UK
[1]epxaad@nottingham.ac.uk, [2] s.leen@nottingham.ac.uk, [3] thomas.hyde@nottingham.ac.uk

Abstract

This paper describes high temperature cyclic elastic-plastic testing of XN40F material for application to the life prediction of superplastic forming (SPF) tools. Cyclic plasticity material constitutive constants are identified from the high temperature tests across the range of 20ºC to 900ºC for representative predicted die conditions. These material constants are implemented within a transient, elastic-plastic-creep, thermo-mechanical analysis method for the die to furnish stress-strain-temperature cyclic data for creep-fatigue life prediction. A simulative thermo-mechanical fatigue (TMF) test, designed to represent the temperature and stress-strain cycling associated with the most damaging phase of the die cycle is presented and shown to give lives consistent with the predicted die lives.

Keywords:
Superplastic forming, plastic shakedown, heating-cooling cycles, part-forming cycles, thermo-mechanical fatigue and creep, major cycle, minor cycle, NLKH, TMF

1 INTRODUCTION

Superplastic forming tools need to withstand high temperature cyclic loading and steady mechanical loading for extended durations and therefore are manufactured (by casting) from specialized alloys, but at the same time numerous additional geometrical complexities result from weight-saving constraints (due for example to weight limitations in industrial plant related to handling capacities) and ruling section requirements for casting. The cost of tool failure is significant and tool life is an important limiting aspect in the SPF process; the SPF process is a high value-added process, rather than a mass production process.

Large SPF tools mainly suffer from distortion due to thermal cycling and high temperature creep. Creep relaxation during forming induces inelastic deformation and distortion of the tool after cooling to the ambient [1]. SPF tool distortion can lead to the forming of inaccurate parts which incurs the expense of repair and replacement of such tools. In addition to distortion, the thermo-mechanical fatigue and fatigue-creep interaction can lead to cracking. Finite element (FE) based simulation of realistic thermo-mechanical conditions is an effective method for analysing realistic large SPF tool behaviour to predict the complex temperature-stress-strain cycles and hence damage and deformation for distortion assessment and hence distortion control or minimisation. Material models are crucial for the credibility of FE predictions and hence the choice of suitable material model is important for numerical simulations.

A comparatively simple uncoupled plasticity–creep material model is investigated here to analyse the thermo-mechanical behaviour of a simplified, representative SPF tool. The salient stresses and strains are developed by thermal gradients during heating, cooling and opening/closing of the press for blank loading and part unloading operations. The cyclic plasticity during temperature transients is modelled using Chaboche non-linear kinematic hardening [4] and power law (Norton) creep is used to model the creep deformation during the dwell period of each forming cycle.

Cyclic plasticity material constitutive constants are identified from the tests across the range of relevant temperatures of 20ºC to 900ºC by varying the strain-ranges and the identification process is carried out for two different strain-rates, corresponding to representative predicted

conditions for SPF dies. The determined constitutive plasticity model is applied with an uncoupled creep model, for the dwell periods during forming cycles, within a previously-established transient thermo-mechanical model of the die to predict the cyclic elastic-plastic-creep behaviour. The effect of using different constitutive constants associated with the different strain-rates on die behaviour is predicted and a bi-linear strain-range partitioning method for creep-fatigue life prediction is applied to predict die life. The die life predictions using the new cyclic material data are compared with previous results. Finally, a simulative thermo-mechanical fatigue test, designed to represent the temperature and stress-strain cycling associated with the most damaging phase of the die cycle is presented and shown to give lives consistent with the predicted die lives.

2 MATERIAL TESTING

An Instron thermo-mechanical fatigue test rig is employed to carry out the high temperature material testing. The test machine uses a servo-electric dynamic loading system and uses an induction coil to achieve the high temperatures required to simulate the die operating conditions. Figure 1 shows the fatigue specimen employed and also the induction coil at a temperature of 900°C with the ceramic-rod extensometer in-situ to effect strain control.

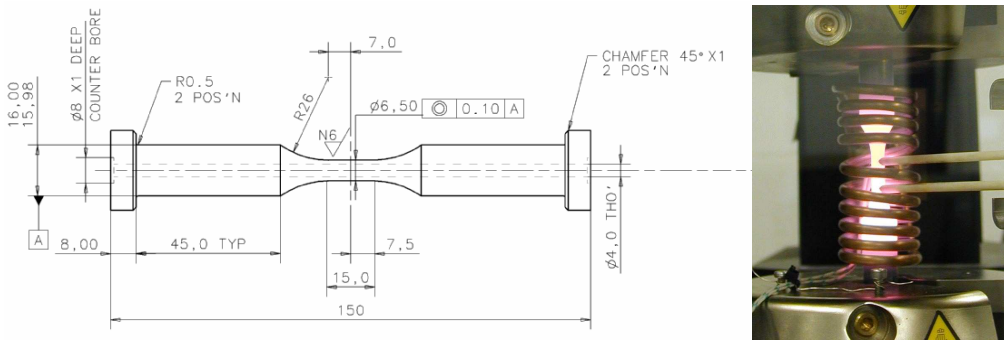

Fig. 1 Geometry of thermo-mechanical fatigue test specimen and induction coil with extensometer.

Temperature uniformity over the gauge length of ±10°C for 200 °C to 900°C has been achieved using careful design of the induction coil. The specified heating and cooling rates of the test machine are 50±10 ºC/sec and 25±10 ºC/sec, respectively. Automated thermal strain compensation and Young's modulus determination to impose the target mechanical strain are implemented within the system according to the ASTM thermo-mechanical fatigue testing standard.

The SPF tool is cast from XN40F material. The composition of XN40F tool material is given in Table 1 [2] while the thermal properties are given in Table 2 [3]. Thermal properties such as thermal conductivity and specific heat at different temperatures are required to predict the thermal histories of the SPF tool. The material data from high temperature tensile tests is shown in Table 3. The tensile tests were carried out for four different temperatures; 20˚C, 500˚C, 700˚C and 900˚C which span the temperature range for the SPF process; the average strain rate applied is 8×10^{-4} s^{-1}. The elongation to failure increases significantly with increasing temperature. Brittle fracture occurs below 700˚C and ductile fracture occurs at 900˚C [5]. Short term tensile tests at lower strain rates of 8×10^{-5} s^{-1} and 8×10^{-4} s^{-1} at 900˚C were carried out to determine the short term creep properties as shown in Table 4.

Table 1. Composition of the SPF tool material XN40F [2]

Elements	C	Ni	Cr	Fe
Weight %	0.35	40.0	20.0	Balance

Table 2. Thermal properties of XN40F material at different temperatures [2].

Thermal conductivity		Thermal expansion		Specific heat	
Temperature [°C]	[W/m/K]	Temperature °C	x10^{-6}[/°C]	Temperature[°C]	[J/kg/K]
20	11	20-100		0	437
500	20	20-500	15.8	500	536
850	26	20-850	17.35	850	603
950	28	20-950	17.7	950	618

Table 3. Monotonic mechanical properties of XN40F material at different temperatures for strain rate of 8×10^{-4}/s [2].

Temperature [°C]	Young's modulus [GPa]	0.2% Yield strength [MPa]	UTS [MPa]	Elongation [%]	$C = \frac{\partial \sigma}{\partial \bar{\varepsilon}^{pl}}$ [MPa]
20	110	172	332	3	6154
500	108	145	320	6	3182
700	104	110	286	16	1213
900	92	107	120	37	36

Table 4. Measured creep behaviour and constants of XN40F material of 900°C [2].

Strain rates [s^{-1}]	Stress [MPa]	A [$MPa^{-n}s^{-1}$]	n
8×10^{-4}	136	9.14×10^{-14}	4.66
8×10^{-5}	83		

Cyclic multiple strain range isothermal tests at 20˚C, 500˚C, 700˚C and 900˚C for two strain rates, 5×10^{-3} s^{-1} and 5×10^{-4} s^{-1}, are carried out here to characterise the temperature-dependent cyclic stress-strain behaviour of the XN40F alloy. Lower strain-ranges were employed for the lower temperatures, consistent with anticipated relevant in-situ conditions. Figure 2 shows the cyclic stress-strain curves obtained from the tests at different temperatures. Table 5 summarises the complete test programme.

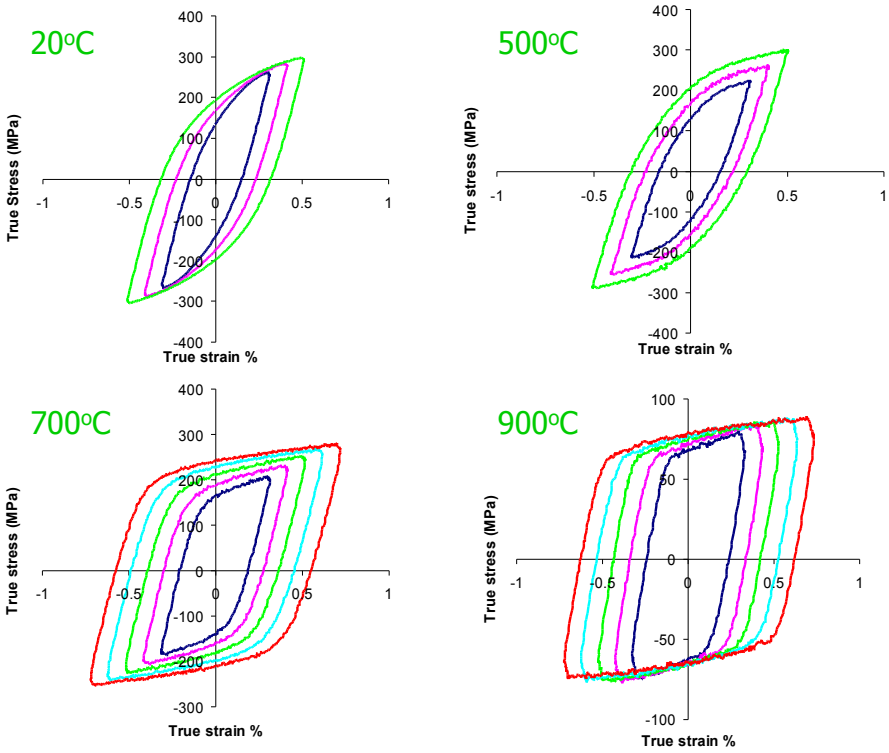

Fig. 2 Measured stabilised stress-strain loops for XN40F for different temperatures and strain-ranges for strain rate of 5×10^{-4} s^{-1}.

3 Identification of material constitutive constants

The material constitutive model employed here is a temperature-dependent, non-linear kinematic hardening (NLKH) model, with uncoupled secondary (Norton) creep during the dwell time at 900ºC. The Ziegler kinematic hardening law within ABAQUS [3] is used to simulate the translation of the yield surface in the stress space, through the back stress, $\boldsymbol{\alpha}$.
The total strain rate is decomposed into elastic and plastic strain rates, as follows:

$$\dot{\boldsymbol{\varepsilon}} = \dot{\boldsymbol{\varepsilon}}_{el} + \dot{\boldsymbol{\varepsilon}}_{pl} \tag{1}$$

with the linear elastic behaviour defined as:

$$\boldsymbol{\sigma} = \mathbf{D}^{el} : \boldsymbol{\varepsilon}^{el} \tag{2}$$

where $\mathbf{D}^{el}$ is the material stiffness matrix and the yield surface is defined by:

$$f(\boldsymbol{\sigma} - \boldsymbol{\alpha}) = k \tag{3}$$

where k is the size of the yield surface and $f(\boldsymbol{\sigma} - \boldsymbol{\alpha})$ is the equivalent Mises stress with respect to the back stress $\boldsymbol{\alpha}$ defined as:

$$f(\boldsymbol{\sigma} - \boldsymbol{\alpha}) = \sqrt{\frac{3}{2}\left(\mathbf{S} - \boldsymbol{\alpha}^{dev}\right) : \left(\mathbf{S} - \boldsymbol{\alpha}^{dev}\right)} \tag{4}$$

where $\boldsymbol{\alpha}^{dev}$ is the deviatoric part of the back stress and $\mathbf{S}$ is the deviatoric stress tensor. The flow-rule equation is:

$$\dot{\boldsymbol{\varepsilon}}_{pl} = \frac{\partial f(\boldsymbol{\sigma} - \boldsymbol{\alpha})}{\partial \boldsymbol{\sigma}} \dot{\bar{\varepsilon}}_{pl} \tag{5}$$

where $\dot{\bar{\varepsilon}}_{pl}$ is the equivalent plastic strain rate defined as follows:

$$\dot{\bar{\varepsilon}}_{pl} = \sqrt{\frac{2}{3}\dot{\boldsymbol{\varepsilon}}_{pl} : \dot{\boldsymbol{\varepsilon}}_{pl}} \tag{6}$$

The size of the yield surface is a function of temperature T and the generalised Ziegler's rule for an-isothermal case is given in the equation below.

$$\dot{\boldsymbol{\alpha}} = C\dot{\bar{\varepsilon}}_{pl}\frac{1}{k}(\boldsymbol{\sigma} - \boldsymbol{\alpha}) - \gamma\alpha\,\dot{\bar{\varepsilon}}_{pl} + \frac{1}{C}\boldsymbol{\alpha}\dot{C} \tag{7}$$

where $C(T)$ is the temperature-dependent hardening modulus of the isothermal uni-axial stress-strain response, $\frac{\partial\sigma}{\partial\bar{\varepsilon}^{pl}}$, measured at different temperatures, $\dot{C}$ is the rate of change of C with respect to temperature and $\gamma\alpha\,\dot{\bar{\varepsilon}}_{pl}$ is a recall term to introduce non-linearity in the evolution law.

Steady state (secondary) creep behaviour is introduced during the (minor cycle) dwell time at the constant temperature of 900ºC using power-law (Norton) creep $\dot{\bar{\varepsilon}}_{cr} = Aq^n t^m$ where A, n and m are temperature dependent material constants, $\dot{\bar{\varepsilon}}_{cr}$ is the uniaxial equivalent creep strain rate, q is the equivalent (von Mises) stress, and t is the total time. A value of m = 0 is assumed here, so that only secondary creep is considered.

Table 5. Summary of high temperature cyclic test programme.

Test No.	Test type	Temperature	Test Specifications	Material parameters
1	Isothermal strain controlled fatigue tests	20ºC, 500ºC, 700ºC, 900ºC	R_ε = -1 $\Delta\varepsilon$ = 0.4%,0.6%, 0.8%,1.2%,1.4% Rates: 5x 10^{-3}/s, 5x 10^{-4}/s	Stabilized Stress-strain loops (k C and γ)
2	TMF OP test with hold period in compression	750 – 900 ºC	R_ε = -1 $\Delta\varepsilon$ = 0.3%, 0.8%, 1.0%, 1.2% Rate: 2.5x 10^{-4}/s Hold period = 120 sec	Life based on 10% load drop
3	TMF OP test	750 - 900ºC	R_ε = -1 $\Delta\varepsilon$ = 0.8%, 1.0%, 1.2% Rate: 2.5x 10^{-4}/s	Life based on 10% load drop
4	Isothermal strain controlled fatigue test without hold period	900ºC	R_ε = -1 $\Delta\varepsilon$ = 0.8%, 1.2% Rate 2.5e-4/s	Life based on 10% load drop
5	TMF OP (Mimic stress-strain loop from FE) With mean strain	750 - 900ºC	$R_\varepsilon \neq$ -1 $\Delta\varepsilon$ = 0.3% Rate =1e-4/s Hold = 120 sec (compression)	Life based on 10% load drop
6	Creep tests	600, 700 and 900ºC	Short term stress control tests to get secondary creep constants	Secondary Creep constants

The material constants for non-linear kinematic hardening (NLKH) are identified from the stabilized hysteresis loops corresponding to different strain amplitudes of multi-strain range isothermal cyclic tests carried out at 20˚C, 500˚C, 700˚C and 900˚C. The material constant k for a particular temperature is determined as the mean of the individual k values for each strain range, which are readily estimated from the stabilised stress-strain loops. The ratio $\frac{C}{\gamma}$ is determined as the asymptotic value of $\frac{\Delta\sigma}{2} - k$ plotted against $\frac{\Delta\varepsilon_p}{2}$, corresponding to the saturated value of back stress. The coefficients C and γ are the identified by fitting the following equation, which represents the NLKH relationship between cyclic stress and strain to the measured cyclic stress-strain data [4]:

$$\frac{\Delta\sigma}{2} - k = \frac{C}{\gamma}\tanh\left(\gamma\frac{\Delta\varepsilon_p}{2}\right) \tag{8}$$

Table 6. Non-linear kinematic hardening material constants of XN40F material at different temperatures from strain controlled cyclic tests.

Strain rate, [s^{-1}]	k [MPa]	C [MPa]	γ	Temperature [˚C]
5×10^{-3}	183	125000	892	20
	160	38000	422	500
	155	21000	300	700
	90	9000	250	900
5×10^{-4}	175	82000	656	20
	154	55000	393	500
	151	32000	267	700
	60	8000	320	900

Figure 3 shows the identification of the coefficients C and γ for the XN40F tool material at 20˚C, 500˚C, 700˚C and 900˚C for the strain rate of 5×10^{-4} s^{-1}. Similarly the material constants are identified for the strain rate of 5×10^{-4} s^{-1}. The identified material constants are summarised in Table 6. The material constants for the strain rate of 5×10^{-4} s^{-1} are used in the SPF tool analysis presented here, although the effect of using the 5×10^{-3} s^{-1} data on the predicted die stress-strain cycle is also presented. Figures 4 and 5 show the comparison of the NLKH material model predictions (using the latter identified constants) with the experimental stabilized loops over the range of temperatures and strain-ranges for the 5×10^{-4} s^{-1} case. The correlation for the 5×10^{-3} s^{-1} case was of equivalent quality. Figure 6 shows the measured and predicted effect of strain-rate on the cyclic stress-strain relationship at 900˚C.

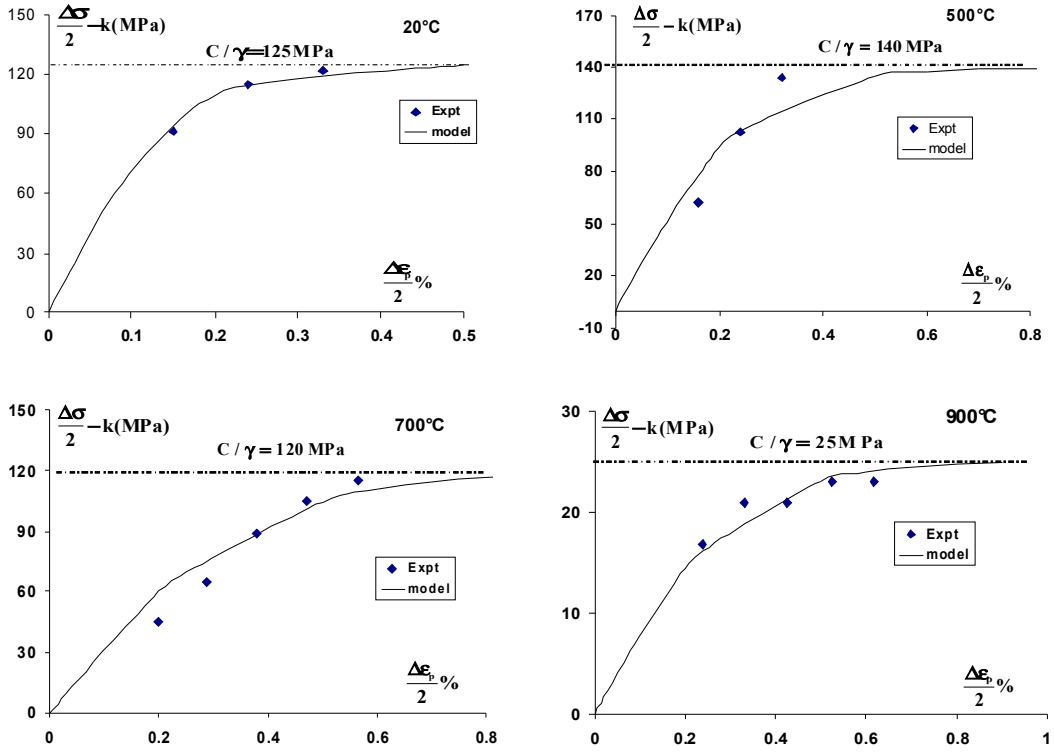

Fig. 3 Identification of coefficients C and γ for strain rate 5×10^{-4} s^{-1}.

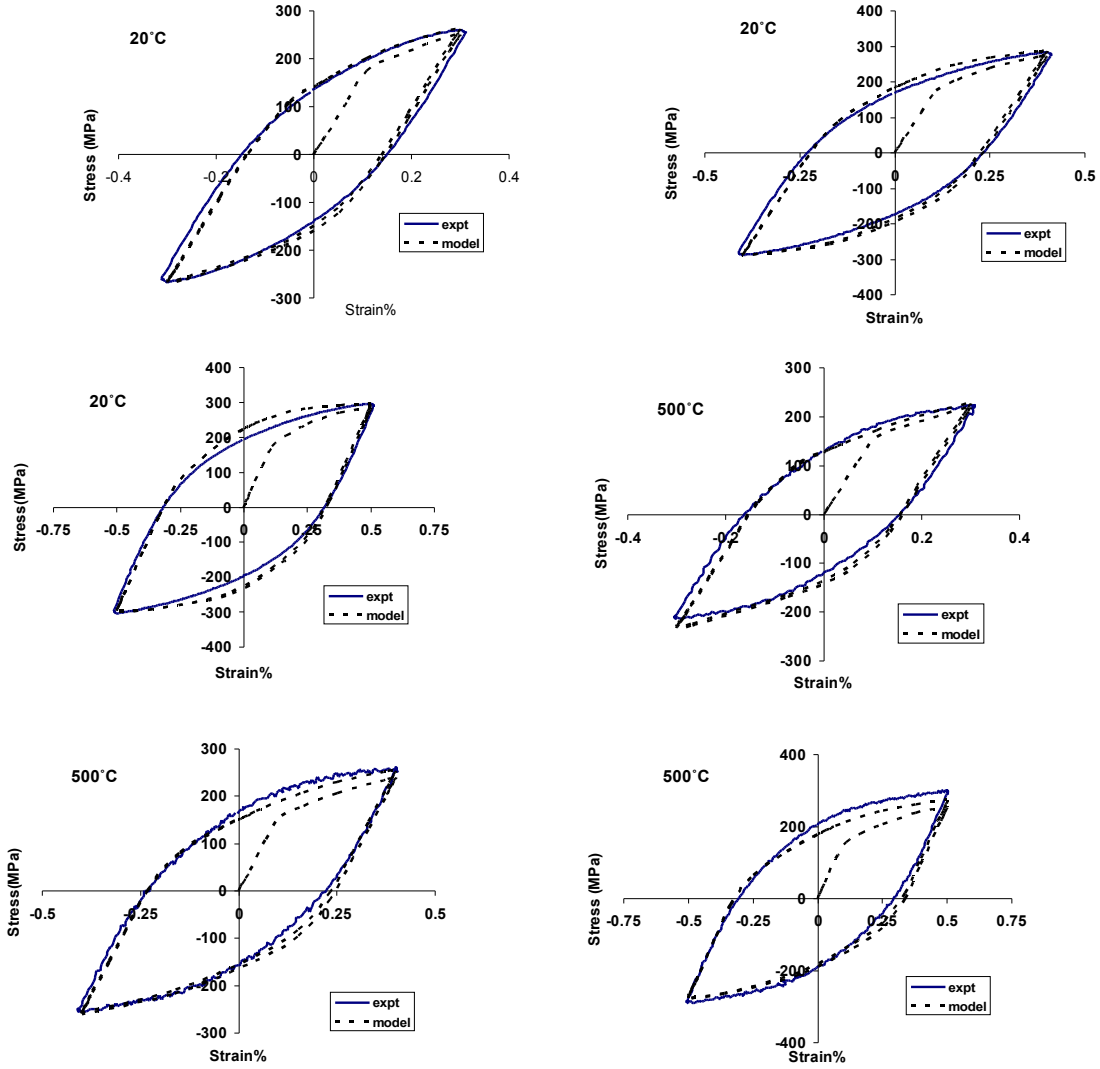

Fig. 4 Validation of identified constitutive constants for different strain-ranges at 20˚C and 500˚C.

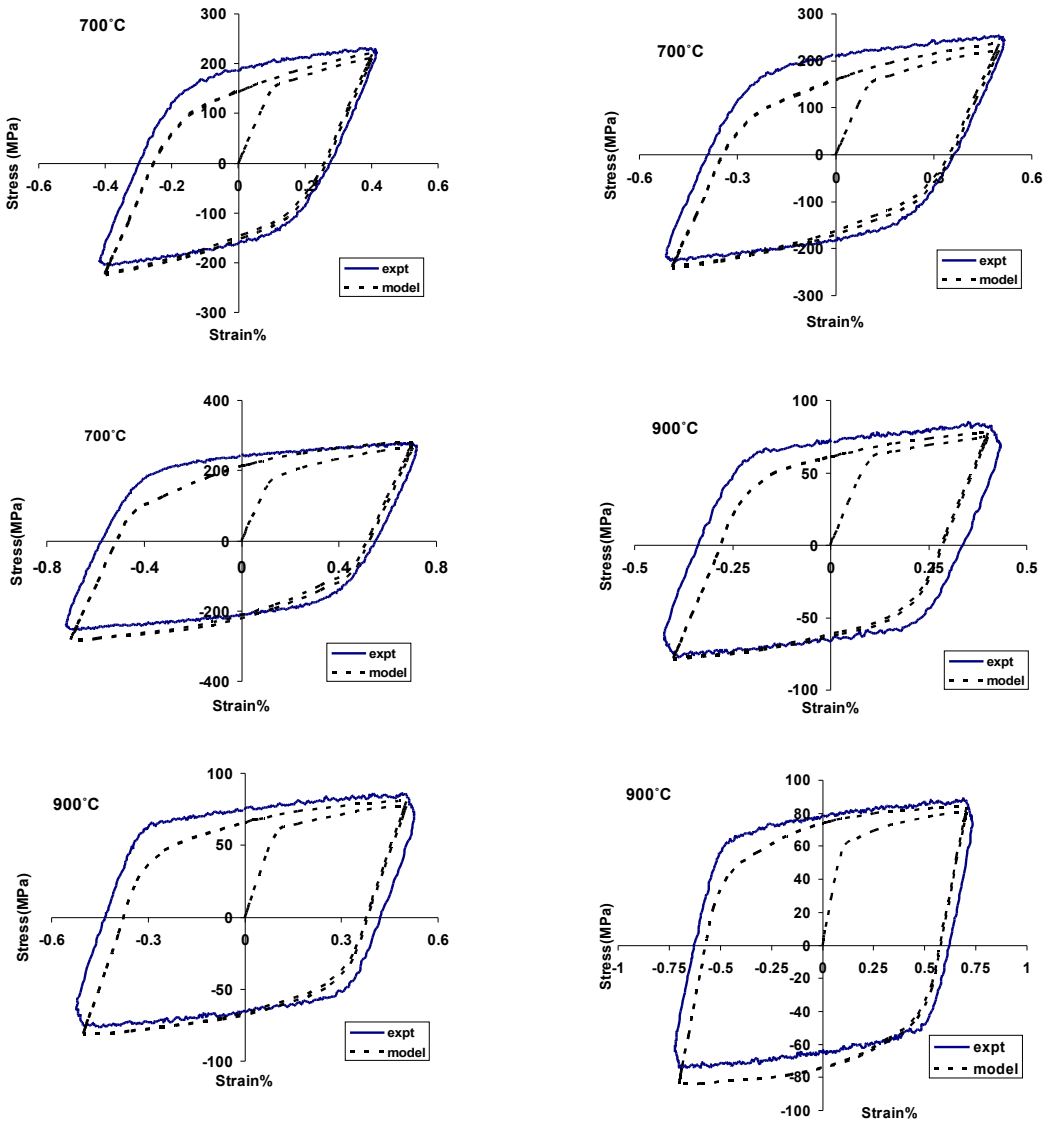

Fig. 5 Validation of identified constitutive constants for different strain-ranges at 700˚C and 900˚C.

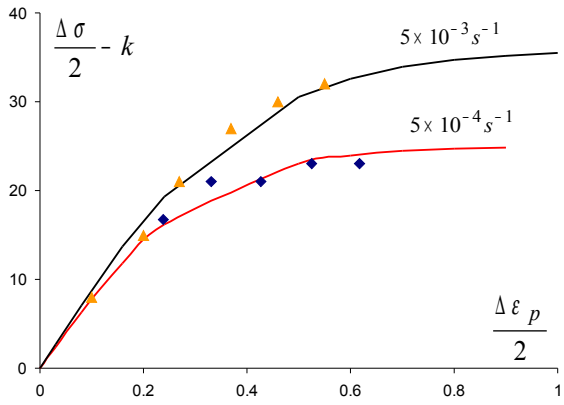

Fig. 6 Effect of strain-rate on cyclic material behaviour and constitutive model at 900˚C.

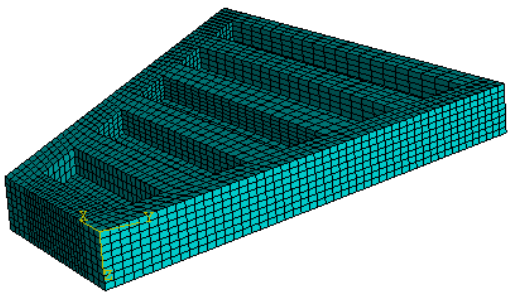

Fig. 7 Underside view of FE model of simplified representative SPF half-tool.

4 THERMO-MECHANICAL ANALYSIS OF SPF TOOL

A realistic SPF tool is represented in a geometrically simplified form, as shown in Figure 7. The main simplifications relate to the omission of local features, such as hangings and alignment lugs, so that the dominant deformation mechanisms are still captured, since the objective here is to address the major cracks observed in real tools. A lower half of the SPF tool is modelled assuming symmetry between the upper and lower tool. The platen-tool contact is defined as a mechanical boundary condition in the FE model. This representative tool has five cavities of 100 mm depth on the underside of the tool. The longest side is approximately 2 m long.

The transient heat transfer methodology used here is the same as that previously validated against the measured heating and cooling experiments for a model die at the University of Nottingham [5]. A realistic SPF thermal history is modelled in the commercial, general-purpose, non-linear FE code, ABAQUS, using conduction, convection and radiation mechanisms.

The SPF tool temperature cycling is complex and is therefore idealised here as divided into two types. The two types are (i) lower frequency cycles, referred to here as major cycles, broadly associated with heating and cooling from ambient, and (ii) higher frequency cycles, referred to here as minor cycles, which are associated with opening and closing of the press doors for blank inserts and removal of formed parts. In reality these cycles are not easy to standardize since they are not automated and are carried out by manual operation. Therefore there can be significant variations in the time periods, in particular, associated with these idealised cycles. Nonetheless, for the purposes of analyses here, they are idealised as follows.

Major cycle

Step 1: The tool is heated in a pre-heat furnace to 500˚C at a controlled rate of 50˚C/hr and then allowed to reach steady state by soaking at 500˚C. The heating process is mainly controlled by conduction with the temperature boundary condition applied to the bottom surface of the tool. The open radiation and free convection mechanisms are also applied with an ambient temperature of 500˚C during the soak time.

Step 2: The tool is transferred to the SPF press in 3 minutes. During this time-period all external surfaces except the top surface of the tool are exposed to the ambient via open radiation and free convection mechanisms.

Step 3: The tool arrives in the SPF press and is heated to 900˚C, again at 50˚C/hr, until a uniform temperature is achieved. This process is again controlled through the conductive heating of the tool via temperature control of the bottom surface nodes.

Step 4: The tool is control-cooled to 500˚C at 50˚C/hr in the SPF press and then removed from the press to cool to ambient temperature via free convection and open radiation.

These four (major cycle) steps are illustrated in Figure 8. Direct heating and cooling to 500˚C in the SPF press is always implemented by controlled temperature variation of the tool bottom surface nodes. The contact with the platen is assumed to be adiabatic.

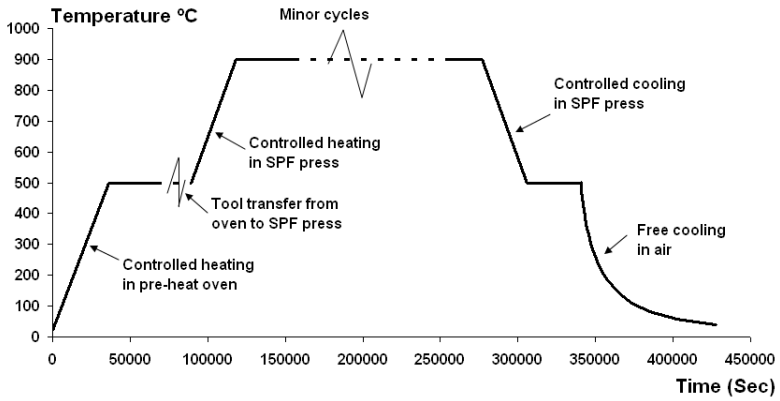

Fig. 8 Schematic of thermal history of SPF tool.

Minor cycle

Step 1: The SPF press is opened to unload the formed component. This consists of allowing the two longest sides of the tool (facing the press doors) to cool via free convection and open radiation with the ambient for a period of 5 minutes.
Step 2: The press is closed again and the tool is heated back to 900˚C.
Step 3: The press is opened again to load the new blank. This again allows the two longest sides to cool via free convection and open radiation for 5 minutes.
Step 4: The press is closed again and the tool is heated back to 900˚C along with the new blank sheet.
Step 5: The tool and the blank temperature is maintained at a constant temperature of 900˚C for 7 hours corresponding to the forming cycle of one component.

Only the lower half of the tool is modelled, as a first approximation and on the basis of approximate symmetry between the two halves. The presence of the upper tool is modelling via the clamping pressure applied along the top edge of the lower tool during the dwell time. The gas pressure during forming is not modelled as the stresses induced by the forming pressure are considered to be negligible [1]. Tool gravity is modelled along with frictional contact (COF = 0.2) between the tool bottom surface and platen where the platen is considered as an analytically rigid surface.
Figure 9 shows the FE-predicted accumulated equivalent plastic strain at the end of three major cycles, each including five minor cycles. Clearly, plasticity is predicted to occur along the top interface edges of the two sides of the tool facing the press doors. The temperature drops along these edges during part loading and unloading (from 900˚C to 744˚C), leading to large temperature gradients. A local co-ordinate system is defined in Figure 9 where the *X* direction (also referred to as 1 direction) is parallel to the edge of the tool on which EL C is present and the *Y*-direction (also referred to as 2-direction) is parallel to the thickness of the tool. The temperature drop to 744ºC along the top interface edges of the two sides of the tool facing the press doors, leads to plasticity deformation, as shown in Figure 9, due to the thermal stresses exceeding the temperature-dependent yield stress.. In fact, the plastic deformation occurs while the temperature drops to 744ºC. The stress is seen to relax from 62 MPa to 8 MPa during the dwell time at 900ºC, due to creep deformation as shown in Figure 10. The constant clamping pressure of 4 MPa across the edges of the top four sides of the tool is also introduced during the dwell time at 900ºC. Figure 10 shows the predicted local σ_{11} stress versus inelastic strain, ε_{11}^{in}, for EL C for three major cycles, including the associated minor cycles. Plastic shakedown is predicted to occur for this combination of stress-strain components, which essentially represents the normal stress-inelastic strain response parallel to

the side of the long side of the die. This suggests that low cycle fatigue is a likely failure mode in this direction.

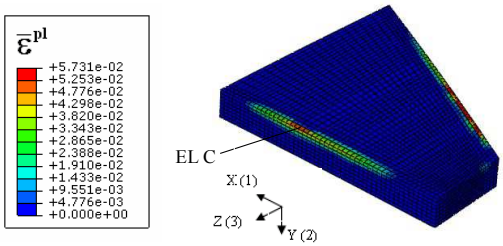

Fig. 9 Equivalent plastic strain distribution at end of 3rd major cycle with local co-ordinate system defined.

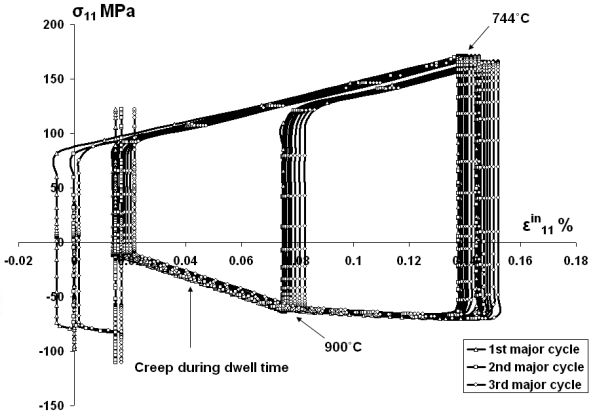

Fig. 10. Local stress versus local inelastic strain for 3 major cycles each including 5 minor cycles.

To understand the minor cycle and anisothermal stress-strain response, the local stress-strain response is plotted for the first minor cycle of the first major cycle in Figure 11, for EL C, Compressive stresses are predicted during the heating-up process to 900ºC, because EL C is on the surface and heats up slower than the bottom surface of the die.

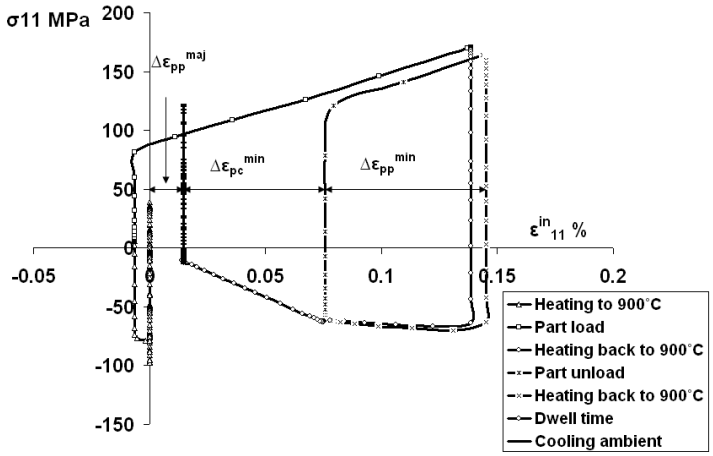

Fig. 11 Local stress versus local inelastic strain for the 1st minor cycle of the 1st major cycle.

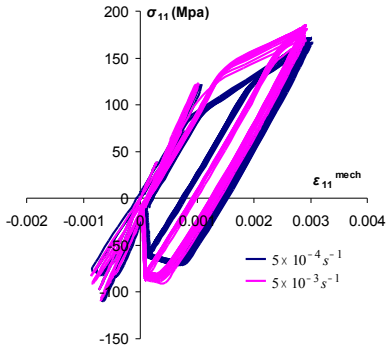

Fig. 12 Effect of different strain-rate constitutive constants on predicted die behaviour.

Very small compressive plastic strain is predicted to occur during this period which comprises slow heating up to 500ºC in the pre-heat oven, tool transfer from the preheat oven to the SPF press and slow heating up to 900ºC in the SPF press. During tool transfer from the pre-heat oven to the SPF press, tensile stress is predicted due to the bottom surface cooling faster than the top surface, which is modelled as being in contact with the upper half of the tool (via an adiabatic boundary condition). During part loading and unloading, a tensile stress is predicted due to the temperature dropping to 744ºC, the bulk of the tool (i.e. away from the doors) remaining at 900ºC. Elastic recovery followed by compressive plastic strain is predicted during re-heat back to 900ºC after every (minor cycle) part load and unload operation. Compressive creep is predicted to follow the compressive plasticity during the dwell time while the stress relaxation is predicted due to creep. Hence, the analyses predict low cycle

fatigue and fatigue-creep interaction damage. Figure 12 shows the effect of the NLKH material constants corresponding to the two strain rates of 5×10^{-4} s^{-1} and 5×10^{-3} s^{-1} on the predicted anisothermal stress-strain cycles for the die. Clearly, the higher strain rate gives higher maximum stress and lower cyclic strain ranges.

5 SPF TOOL LIFE PREDICTION

Shang [6] has proposed a bi-linear creep-fatigue interaction approach for the present XN40F die material. From the finite element modeling (Fig 11), it can be seen that the SPF tool experiences both $\Delta\varepsilon_{pp}$ and $\Delta\varepsilon_{pc}$ cyclic inelastic strain ranges, i.e. cyclic strain ranges with plastic strain reversed by plastic strain ($\Delta\varepsilon_{pp}$) and cyclic strain ranges with plastic strain reversed by creep strain ($\Delta\varepsilon_{pc}$). Associated with these are two damage components, $D_{pc} = \frac{1}{N_{pc}}$ and $D_{pp} = \frac{1}{N_{pp}}$, which represent the damage per cycle associated with $\Delta\varepsilon_{pp}$ and $\Delta\varepsilon_{pc}$, respectively, and where N_{pp} is the number of cycles of $\Delta\varepsilon_{pp}$ to failure and N_{pc} is the number of cycles of $\Delta\varepsilon_{pc}$ to failure. The bi-linear damage summation equations, as shown in Figure 13, are as follows:

$$\alpha\frac{N_f}{N_{pp}} + \frac{N_f}{N_{pc}} = 1 \qquad \text{for } \frac{N_f}{N_{pp}} < \frac{N_f}{N_{pc}} \tag{9}$$

where N_f is the number of combined cycles to failure and where α is a constant greater than 1.

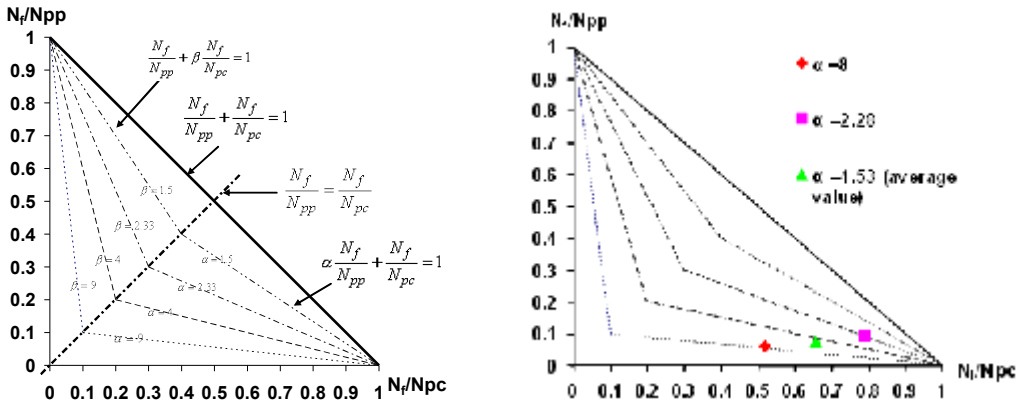

(a) (b)

Fig. 13 Bi-linear strain range partitioning: (a) schematic plot of bi-linear damage assumption approach and (b) measured α values from combined creep-fatigue tests [2, 6].

These equations can be further expanded using Miner's rule to linearly combine major and minor cycle damage, as follows:

$$N_f\left[\alpha\left(\frac{1}{N_{pp}^{maj}} + \frac{2n}{N_{pp}^{\min}}\right) + \left(\frac{1}{N_{pc}^{maj}} + \frac{n}{N_{pc}^{\min}}\right)\right] = 1 \tag{10}$$

where n is the number of minor cycles in a major cycle. A typical value of n = 20, which is representative of industrial practice for the present application, is considered here for predicting the number of major cycles. The total number of minor cycles is $2n$ to take into account the fact that the press doors are opened and closed separately for blank sheet loading and part unloading operations. Strain-controlled fatigue and fatigue-creep interaction tests on

XN40F material were carried out at 700ºC and 900ºC by Shang [6] and the resulting cyclic strain-life equations at 900ºC are employed here in the bilinear strain-range partitioning approach, as follows:

$$N_{pp}(\Delta\varepsilon_{pp})^{1.346} = 1.745 \quad (11)$$

$$N_{pc}(\Delta\varepsilon_{pc})^{1.518} = 0.462 \quad (12)$$

Additional tests at 900ºC, specially devised to simulate the interaction between $\Delta\varepsilon_{pp}$ and $\Delta\varepsilon_{pc}$ strain ranges for the die, were employed by Shang [6], to show that $\frac{N_f}{N_{pp}} < \frac{N_f}{N_{pc}}$ for the die material and to identify the relevant value of α for Equation 90, as shown in Figure 13b. The resulting mean value of α = 4.53 is employed here. Figure 12 also shows the inelastic strain ranges $\Delta\varepsilon_{pp}^{\min}$ and $\Delta\varepsilon_{pc}^{\min}$. $\Delta\varepsilon_{pp}^{maj}$ and $\Delta\varepsilon_{pc}^{maj}$ are negligible in the present case.

Figure 14 shows the typical strain and temperature loading history used for the out-of-phase (OP) TMF tests. Figure 15 shows the resulting stabilized anisothermal stress-strain loop for the same loading conditions and Figure 16 shows that the corresponding FE-predicted response, based on the isothermally-identified material constants of Table 6, give reasonable agreement with the test data.

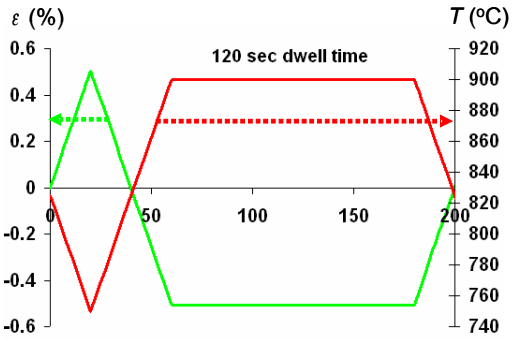

Fig. 14 Typical imposed strain-temperature cycle for simulative TMF test.

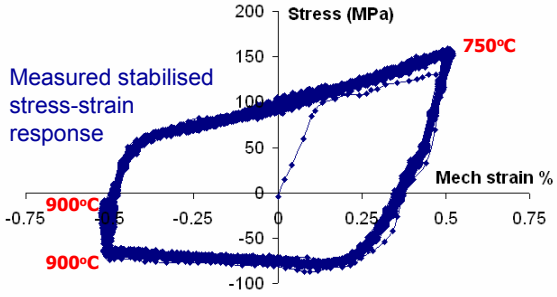

Fig. 15 Typical results from simulative TMF test for $\Delta\varepsilon$ = 1 %.

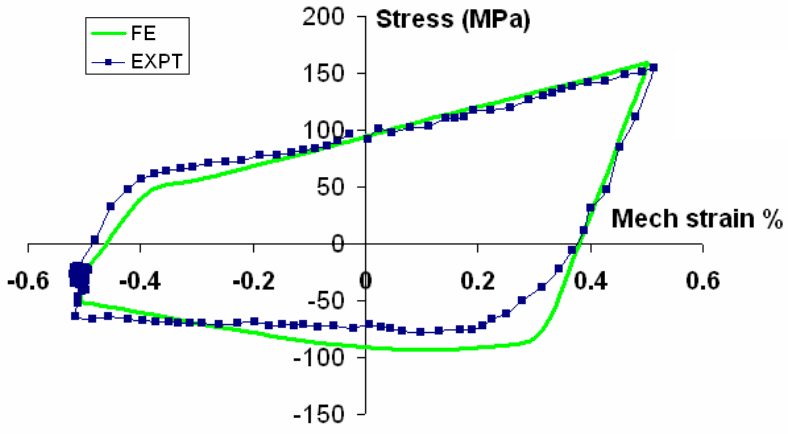

Fig. 16 Comparison of FE-predicted and measured stabilised cyclic stress-strain response for simulative cycle ($\Delta\varepsilon$ = 1 %.)

Based on the results of Figure 12, the same OP TMF test (with hold period of 120 s) with $\Delta\varepsilon$ of 0.3 %, is considered to be 'simulative' of the most damaging phase of the die thermo-

mechanical loading history, viz. the temperature variations associated with the open/closing of the die for insertion/removal of sheet material.
Table 7 summarises the creep-fatigue life predictions from the bi-linear strain range partitioning method, using both monotonic data and stabilised cyclic data, along with the life prediction from the simulative OP TMF test. The predicted creep-fatigue life using the cyclic data (NLKH model) is lower than using the monotonic data (linear kinematic hardening) presented in previous work done by the authors [9].

Table 7. Predicted and 'simulative' fatigue-creep life (major cycles).

Monotonic data	Cyclic data	Simulative OP TMF test for die
178	156	104

6 CONCLUSION

- Isothermal cyclic elastic-plastic characterisation of XN40F under representative strain range, temperature and strain-rate conditions has been presented
- The test data has permitted identification of non-linear kinematic hardening constants across the relevant range of temperatures
- The identified isothermal constants have been validated against the cyclic tests and show reasonable correlation with the largest discrepancies occurring at the high temperatures, due presumably to the omission of rate-dependent effects
- A 'simulative' thermo-mechanical test for the critical damaging phase of part removal-insertion shows good correlation with the predicted die life
- Interpolation with respect to temperature using isothermal NLKH data and creep data within the anisothermal FE analysis is shown to give close correlation with the measured anisothermal stress-strain cycles from an out-of-phase thermo-mechanical fatigue test.
- The use of cyclic data predicts only slightly lower creep-fatigue lives than monotonic data for the material and loading cases considered here
- Future work should address the implementation of (i) a unified cyclic viscoplasticity model, e.g. [10], (ii) anisothermal damage accumulation or life prediction methods and (iii) validation against a realistic die geometry or a representative die geometry, e.g. small-scale dies.

ACKNOWLEDGEMENTS

The authors wish to thank Ian Leaver and John Chippendale of BAE Systems, Salmesbury for helpful discussions. The first author would also like to thank BAE Systems for funding. Thanks also to Mr Chris Hyde and Mr Tom Buss for research on the optimum coil configuration and TMF testing.

REFERENCES

[1] Gao, C.Y., Lours, P., Bernhart, G., *Thermomechanical stress analysis of superplastic forming tools*, Journal of Materials Processing Technology, 169, 2005, 281-291
[2] Shang, J. *Thermo-mechanical life assessment of superplastic forming tools,* PhD Thesis, University of Nottingham, September 2005.
[3] ABAQUS User and Theory Manuals, Version 6.5, HKS Inc., Rhode Is., US, 2004
[4] Lemaitre J., Chaboche J., *Mechanics of solid materials,* Cambridge University press, 1990.
[5] Shang, J., Leen, S.B, and Hyde, *T.H., Finite element based methodology for predicting the thermomechanical behaviour of superplastic forming tools*. Proc. IMechE, Part L: J. Materials: Design and Applications*,* 2006**,** 220(L3), 113-123.

[6] Shang, J., Leen, S.B, and Hyde, T.H., *Finite element based life prediction for high temperature cyclic loading of a large superplastic forming die*, J. Strain Analysis, Vol. 41, no.8. 2006, 539-559.

[7] Kapoor, A., *A re-evaluation of the life to rupture of ductile metals by cyclic plastic strain*, Fatigue & Fracture of Engineering Materials and Structures, 17 (2), 1994, p 201–219.

[8] Deshpande, A.A., Leen, S. B. and Hyde, T. H., *Finite element based predictions of life limiting behaviour for a large SPF tool*, Materialwissenschaft und Werkstofftechnik, 39(4-5), 2008, 309-316

[9] Deshpande, A., Leen, S.B., Hyde, T.H., *Progressive distortion behaviour of large SPF tool under thermo-mechanical fatigue and fatigue-creep interactions*. 19th International Conference on Superplastic Forming, AeroMat 08, Austin, Texas, USA, June 23-26, 2008.

[10] Bernhart, G., Nazaret, F., Martinier, A., *Design of SPF dies based on advanced material behaviour models*, Materials Science Forum, Vols 447-448, 2004,123-130.